

A Speed Sensor Fault-Tolerant Control of the CPPM Machine for Electric Vehicle

Zheran Li¹, Yesong Li¹, Xinhua Li²

¹*Department of Control Science and Engineering, Automation Institute, Huazhong University of Science and Technology, Hubei, China*

²*School of Electrical & Electronic Engineering, Hubei University of Technology, Hubei, China, lizheran@hust.edu.cn*

Abstract—A speed sensor fault-tolerant control (FTC) strategy for electric vehicle is proposed in electric vehicles using a consequent-pole permanent-magnet (CPPM) machine. In order to obtain good FTC performance at low speed region, a HF voltage injection method is proposed to detect the rotor position from the magnetic saliency. This magnetic saliency of a CPPM machine is analysed by the finite-element analysis (FEA), and the high-frequency (HF) impedances are measured to confirm the saliency. At high speed range, the extended-electromotive force (EMF) method is applied when the failure of the speed sensor is detected. The speed sensor FTC strategy is verified effective by experimental results on a 25kW CPPM machine at different operating conditions. The reliability is enhanced and smooth transition to the fault-tolerant operation is realized.

Index Terms—CPPM machine, electric vehicle, speed sensor fault-tolerant control, high-frequency voltage injection, extended-EMF.

I. INTRODUCTION

Permanent magnet synchronous machine (PMSM) based propulsion system is widely used in electric vehicles (EVs) due to its high torque capability and power density [1]. However, flux-weakening in PMSM is achieved by armature reaction to demagnetize the magnets. This approach results in significant power losses and may lead to irreversible demagnetization of permanent magnets [2].

The hybrid excitation synchronous machine (HESM) is proposed to avoid the above-mentioned problems [2]–[5]. The consequent-pole permanent-magnet (CPPM) machine is a special type of HESM that combines the fixed excitation generated by the permanent magnet with the variable flux provided by an excitation winding located in the stator. Adjusting the direction and magnitude of the excitation current can change the combined flux easily.

In the automotive context, the reliability and the continuous operation capability are important issues. The current, voltage, and speed sensors are required to work properly during the operation of the propulsion control. In the EV case, the

resolver is extensively chosen due to its superiority in wide temperature range and high humidity and other harsh environment conditions. Nevertheless, the speed sensor is less reliable than the electrical sensors due to the mechanical coupling. The fault conditions such as intermittent connection or complete outage may lead to danger of the drive system immediately, if no proper actions are taken. The resolver fault detection can be accomplished by the resolver-to-digital converter (RDC) with a proper configuration. Therefore, the speed sensor reconfiguration scheme must be investigated to obtain a fault-tolerant operation in EVs. Extensive research has been carried out [6]–[12]. A FTC of induction motor with maximum-likelihood voting is introduced in [8]. The virtual speed sensors implemented by adaptive observer and extended Kalman filter work with the encoder simultaneously. Reference [9] proposed a position estimation method based on an unknown input observer without voltage knowledge. Reference [10] presents a FTC with automatic reconfiguration scheme. Indirect vector controller, sensorless vector controller, sensorless scalar controller and open-loop Volt/Hertz controller are chosen by a fault detector. Reference [11] studies the sensor fault detection and isolation method in interior-PMSM based on the extended Kalman filter, in which all the sensor faults are detected and isolated. However, the implementation of the extended Kalman filter is difficult and the performance will be deteriorated at very low speed due to parameters variations [12].

In this context, a FTC strategy for a CPPM machine in EV propulsion is proposed in case of speed sensor failure. The speed sensor FTC strategy is implemented combining the HF voltage injection method with the extended EMF method. The experimental results on a 25 kW CPPM machine verify the effectiveness of the proposed speed sensor FTC strategy.

II. MATHEMATICAL MODEL OF THE CPPM MACHINE

A. Description of the CPPM Machine

The basic construction of a CPPM machine is shown in Fig. 1. The armature core is divided into two parts with an excitation winding in the center. The rotor is divided into two also.

The permanent magnets provide a fixed air-gap flux. When

Manuscript received September 3, 2013; accepted December 13, 2013.
This research was funded by a grant (No. 2012ZX04001-012) from The National Major Science and Technology Projects of China.

the DC current is injected into the excitation winding, another flux is generated from one iron pole to the next one. These two parts establish the main flux of the CPPM machine.

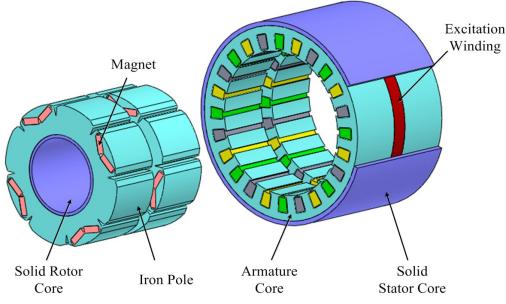


Fig. 1. Basic construction of CPPM machine.

B. Fundamental Model of the CPPM Machine

In the actual rotor reference, the flux linkage equations of the CPPM machine can be described as [13]:

$$\begin{cases} \mathbb{E}_d^r = L_d i_d^r + M_{sf} i_f + \mathbb{E}_{pm}, \\ \mathbb{E}_q^r = L_q i_q^r, \\ \mathbb{E}_f = 1.5 M_{sf} i_d^r + L_f i_f, \end{cases} \quad (1)$$

where superscripts ‘r’ represents the variable in actual rotor reference frame. \mathbb{E}_d^r and \mathbb{E}_q^r are the d-axis and q-axis flux respectively. \mathbb{E}_f is the excitation flux. L_d and L_q are the d-axis and q-axis inductance respectively. L_f is the excitation inductance. i_d^r and i_q^r are the d-axis and q-axis current respectively. i_f is the excitation current. M_{sf} is the inductance between d-axis and excitation windings. \mathbb{E}_{pm} is the permanent magnet flux.

Then, the voltage components are expressed as:

$$\begin{cases} u_d^r = R_s i_d^r + \dots L_d i_d^r + \dots M_{sf} i_f - \tilde{S}_r L_q i_q^r, \\ u_q^r = R_s i_q^r + \dots L_q i_q^r + \tilde{S}_r (L_d i_d^r + M_{sf} i_f + \mathbb{E}_{pm}), \\ u_f = R_f i_f + \dots L_f i_f + 1.5 \dots M_{sf} i_d^r, \end{cases} \quad (2)$$

where u_d^r and u_q^r are the d-axis and q-axis voltage respectively. u_f is the excitation voltage. R_s and R_f are the stator and excitation resistance respectively. \tilde{S}_r is the electric angular velocity. \dots is the differential operator.

The torque is expressed as

$$T_e = 1.5 N_p \left[(\mathbb{E}_{pm} + M_{sf} i_f) i_q^r + (L_d - L_q) i_d^r i_q^r \right], \quad (3)$$

where T_e is the electromagnetic torque. N_p is the number of pole pairs.

III. SPEED SENSOR FAULT-TOLERANT CONTROL

A momentary lack of rotor position information may lead

to overcurrent due to decoupling failure [14]. In this situation, the rotor position must be reconstructed by a proper rotor position estimation method. A HF voltage injection method is applied at low speed region to avoid the poor performance caused by the low magnitude of the back-EMF. Furthermore, an extended EMF method is performed at high speed region to achieve a speed sensor fault-tolerant operation in the entire speed region.

A. HF Voltage Injection Method

At low speed region, the frequency of the injected voltage is much higher than the rotor electric angular frequency. The HF resistance terms, the dq-axis cross coupling terms and back-EMF terms can be neglected [15]. Thus, the simplified HF voltage equations are given as:

$$\begin{cases} u_{dh}^r = \dots L_{dh} i_{dh}^r + \dots M_{sf} i_{fh}, \\ u_{qh}^r = \dots L_{qh} i_{qh}^r, \\ u_{fh} = \dots L_f i_{fh} + 1.5 \dots M_{sf} i_{dh}^r, \end{cases} \quad (4)$$

where the subscript ‘h’ represents HF component of the variables.

Because the HF voltage is not injected into the excitation winding, the cross coupling component between the d-axis and excitation winding in (4) can be decoupled as:

$$\begin{cases} u_{dh}^r = \dots i_{dh}^r \left(L_{dh} - \frac{1.5 M_{sf}^2}{L_f} \right), \\ u_{qh}^r = \dots L_{qh} i_{qh}^r. \end{cases} \quad (5)$$

Due to the special structure of the CPPM machine, the self-inductance of the excitation winding L_f is much larger than M_{sf} . Thus, the cross coupling component can be neglected. Therefore, (5) can be simplified as:

$$\begin{cases} u_{dh}^r = j \tilde{S}_c L_{dh} i_{dh}^r = z_{dh} i_{dh}^r, \\ u_{qh}^r = j \tilde{S}_c L_{qh} i_{qh}^r = z_{qh} i_{qh}^r, \end{cases} \quad (6)$$

where j is the operator ($1 \angle f/2$). z_{dh} and z_{qh} are the d-axis and q-axis impedance respectively.

The rotor position error is defined as

$$\tilde{\theta} \equiv \theta - \hat{\theta}, \quad (7)$$

where θ is the rotor position. Superscripts ‘ $\hat{\cdot}$ ’ represent the variable in estimated rotor reference frame. Superscripts ‘ $\tilde{\cdot}$ ’ represent the error of variable between actual rotor reference and estimation rotor reference.

Transforming (6) into the estimation rotor reference frame with $\tilde{\theta}$, the resultant HF current can be expressed as:

$$\begin{cases} \hat{i}_{dh}^r = \frac{1}{z_{dh} z_{qh}} \left[(z_{avg} - z_{diff} \cos 2\tilde{\theta}) \hat{u}_{dh}^r - (z_{diff} \sin 2\tilde{\theta}) \hat{u}_{qh}^r \right], \\ \hat{i}_{qh}^r = \frac{1}{z_{dh} z_{qh}} \left[(-z_{diff} \sin 2\tilde{\theta}) \hat{u}_{dh}^r + (z_{avg} + z_{diff} \cos 2\tilde{\theta}) \hat{u}_{qh}^r \right], \end{cases} \quad (8)$$

where:

$$\begin{cases} z_{avg} = \frac{z_{dh} + z_{qh}}{2}, \\ z_{diff} = \frac{z_{dh} - z_{qh}}{2}. \end{cases} \quad (9)$$

Equation (8) shows that the HF currents contain the rotor position estimation error when the HF voltage is injected. Because the HF components of the dq-axis are completely decoupled, the injection of HF voltage into d-axis will not generate the torque ripples. Therefore, the HF current response can be obtained as (11) when the HF voltage as (10) are injected into

$$u_{dh}^{\wedge} = u_{inj} \cos \tilde{S}_c t, \quad (10)$$

where \tilde{S}_c is the carrier signal frequency, u_{inj} is the carrier signal magnitude:

$$\begin{cases} \hat{i}_{dh}^{\wedge} = \frac{u_{inj} \cos \tilde{S}_c t}{z_{dh} z_{qh}} (z_{avg} - z_{diff} \cos 2\tilde{\theta}_n), \\ \hat{i}_{qh}^{\wedge} = \frac{u_{inj} \cos \tilde{S}_c t}{z_{dh} z_{qh}} (-z_{diff} \sin 2\tilde{\theta}_n). \end{cases} \quad (11)$$

A signal processing shown in Fig. 2 is applied to obtain $\tilde{\theta}_n$ from (11). A second-order Butterworth band-pass filter (BPF) is applied to extract the HF current. Because the HF voltage injection method is only adopted at low speed region, the pass band of the BPF is set to [900 Hz, 1100 Hz] with a 1 kHz injection voltage. The BPF can be described by following differential equation

$$H_{BPF}(z) = 0.0592 \frac{1 - z^{-2}}{1 - 1.5252z^{-1} + 0.8816z^{-2}}. \quad (12)$$

Then, a multifunction with $\sin(\tilde{\theta}_n t)$ and a first-order low-pass filter (LPF) is used to extract the fundamental signal containing $\tilde{\theta}_n$ from \hat{i}_{qh}^{\wedge} . The cut-off frequency is set to 500 Hz considering the delay and stop band attenuation. The LPF can be described by following differential equation

$$H_{LPF}(z) = 0.1367 \frac{1 + z^{-1}}{1 - 0.7266z^{-1}}. \quad (13)$$

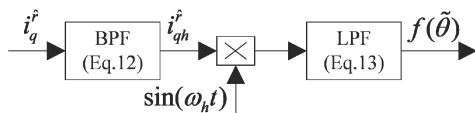


Fig. 2. Signal processing of the HF voltage injection.

If $\tilde{\theta}_n$ is sufficiently small, the resultant signal as (14) can be used to track the rotor position and speed by the phase locked loop (PLL) observer

$$f(\tilde{\theta}_n) = -\frac{u_{inj}(L_{dh} - L_{qh})}{4\tilde{S}_c L_{dh} L_{qh}} \sin 2\tilde{\theta}_n \approx K_n \tilde{\theta}_n. \quad (14)$$

Equation (14) shows that the position error can be obtained if the significantly difference between L_{dh} and L_{qh} is existed. In order to verify this magnetic saliency of the CPPM machine, a FEA approach and measurement of HF impedances of the CPPM machine are carried out.

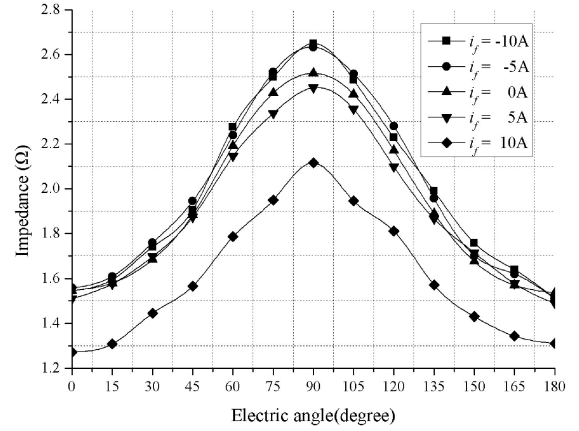


Fig. 3. High-frequency impedances of the CPPM machine under various excitation currents (experimental results, 35 V–1000 Hz).

Fig. 3 presents the measurement results of HF impedance characteristics of the CPPM machine according to the method described in [16]. The HF voltage is injected from 0 degree (d-axis) to 90 degree (q-axis) and to 180 degree (negative d-axis). The results indicate that the d-axis HF impedance is significantly smaller than the q-axis one under various excitation currents. When the excitation current increases, a larger decrement of q-axis HF impedance is obtained.

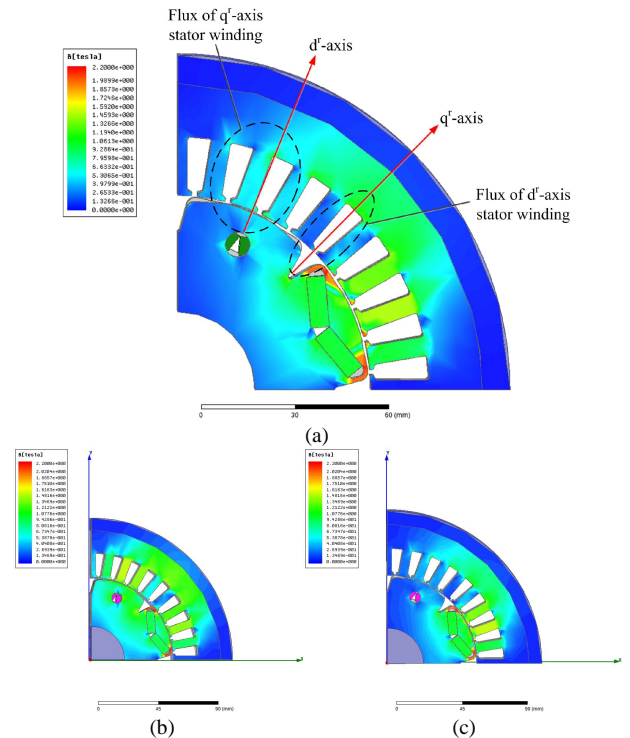


Fig. 4. Distribution of the flux in a CPPM machine under various excitation currents: (a) no excitation current, (b) magnetizing with 1000 ampere-turn, (c) demagnetizing with 1000 ampere-turn.

The flux distributions shown in Fig. 4 are obtained to clarify the magnetic saliency of the CPPM machine. The windings and the flux generated by them are orthogonal as

u_p , the HF voltage should be cancelled to avoid disturbances.

D. Switching Method for the Speed Sensor FTC

The actual rotor position and speed are obtained from the resolver for a proper operating. When the speed sensor fault signal generated by RDC is detected, the rotor position and speed should be obtained from the speed sensor FTC instead. The PLL observer is implemented by a PI controller and an integrator. An incorrect initial state of the PI controller may lead to position estimation failure. Therefore, the PI controller should be controlled by the speed sensor fault signal. When the system is working properly, the integral term is replaced by the actual rotor speed, and the proportional term is ignored. Thus, the output of the PI controller follows the actual rotor speed. When the speed sensor fault signal is detected, the combined position error $\tilde{\theta}_{com}$ is inputted into the PI controller and an integrator to track the rotor speed and position. Thus, the initial state of the PI controller can be obtained properly when the failure of speed sensor occurs.

IV. EXPERIMENTAL RESULTS

To verify the effectiveness of the proposed speed sensor FTC strategy, the control functions were implemented according to Fig. 7 in a control board, which was constructed by the TMS320F2808 digital signal processor. Tamagawa TS2225 resolver and Analog Device AD2S1210 RDC were adopted to obtain the rotor position and speed. The experimental test was performed on a 25-kW CPPM machine, employing a dynamometer as the mechanical load. The parameters of the CPPM are listed in Table I.

TABLE I. THE CPPM MACHINE PARAMETERS.

Parameters	Value	Unit
Rated voltage	220	V
Rated power	25	kW
Rated speed	3000	r/min
Rated excitation current	10	A
Number of pole pairs	4	-
Stator resistance	0.0163	
Excitation winding resistance	1.3702	
d-axis inductance	0.24	mH
q-axis inductance	0.35	mH
Mutual inductance between d-axis and excitation windings	1.5	mH
Self-inductance of excitation winding	39.5	mH
Flux linkage established by magnets	0.058	Wb

The experimental setup for the drive system is shown in Fig. 6.

In the experiment, the input voltage of the driver was limited to 110 V; thus, the rated speed was converted to 1500 r/min. The current loop and rotor position estimation were implemented with a 100- μ s sampling time, and the speed loop was set to 300- μ s. The injection condition was selected as 35 V–1000 Hz. u_p and u_{low} were set to 600 r/min and 400 r/min, respectively.

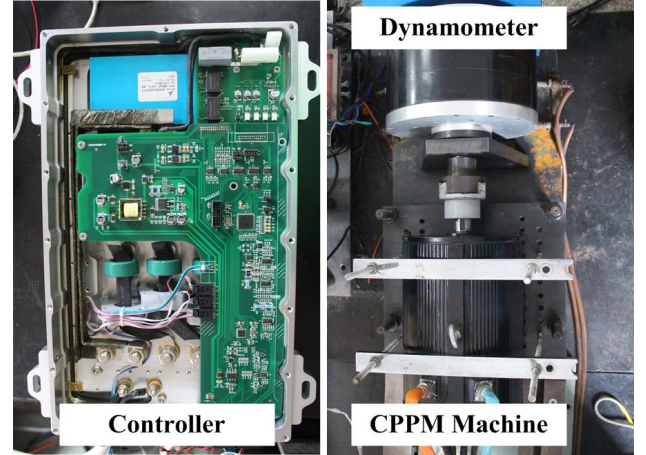


Fig. 6. Experimental setup.

A. Speed Sensor FTC at Low-speed Region

Fig. 8 presents the experimental results for the HF voltage injection method at 100 r/min with 50 % rated load. The results show that the proper rotor position is estimated, and a stable operation of the CPPM machine can be obtained without using the speed sensor.

A series of tests under different speed and load conditions is carried out to evaluate the dynamic performance in case of speed sensor failure and reconstruction. Fig. 9 presents the dynamic response when the speed sensor failure occurs at 100 r/min with 75 % rated load. At 0.43 s, the speed sensor failure is detected. The HF voltage is injected immediately. The rotor position is reconstructed quickly after a short transient process. The position error increases based on the amount of load [17]. However, the stability of the system is guaranteed. The results confirm the effectiveness of the speed sensor FTC strategy at low-speed region.

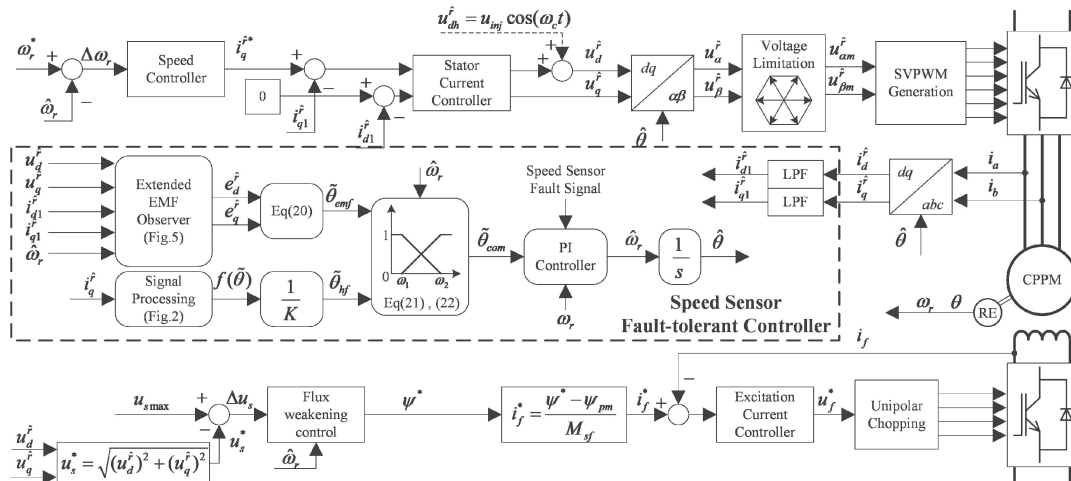


Fig. 7. Block diagram of the CPPM machine drive system.

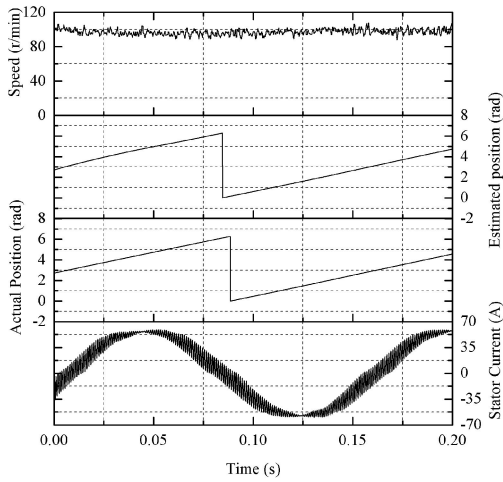


Fig. 8. HF voltage injection and position estimation at 100 r/min with 50 % rated load.

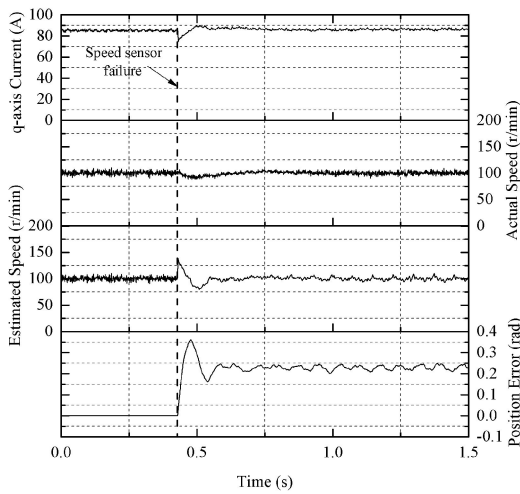


Fig. 9. System dynamic at 100 r/min with 75 % rated load.

B. Speed Sensor FTC at High-speed Region

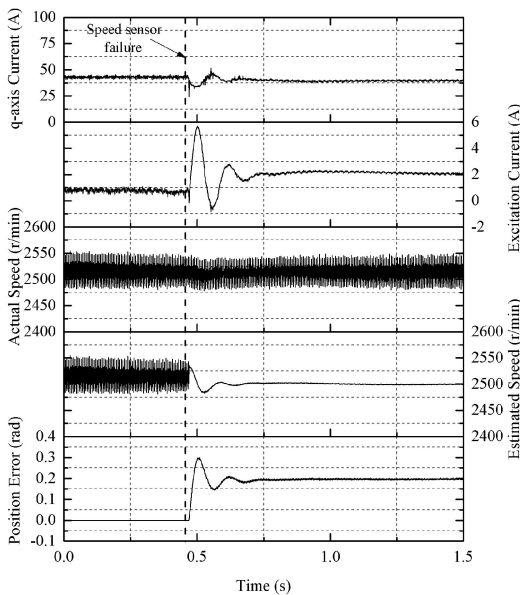


Fig. 10. System dynamic at 2500 r/min with 30 % rated load.

Fig. 10 presents the dynamic response of the CPPM machine when speed sensor failure occurs at 2500 r/min with 30 % rated load. The extended EMF method is used to track the rotor position when the speed sensor failure occurs. The fixed parameters of the CPPM machine applied in the FTC

strategy introduce some position error. When the position error is greater than zero, a negative d-axis current is obtained in actual rotor reference frame. The objective flux, which should be weakened in the flux-weakening region, is partially weakened by the negative d-axis current. Thus, a higher excitation current response is obtained when the speed sensor failure occurs.

C. Speed Sensor FTC at Medium-speed Region

Fig. 11 presents the dynamic response of the CPPM machine when speed sensor failure occurs at 500 r/min with 75 % rated load. The error signals from HF voltage injection method and extended EMF method are combined in this speed region. The position error is reduced due to the combination of two position estimation method.

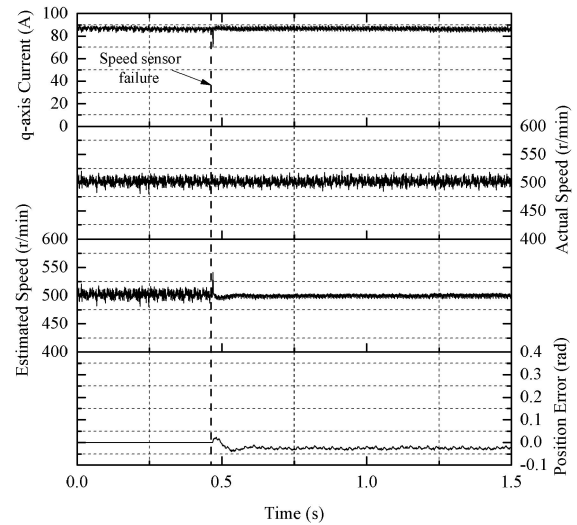


Fig. 11. System dynamic at 500 r/min with 75 % rated load.

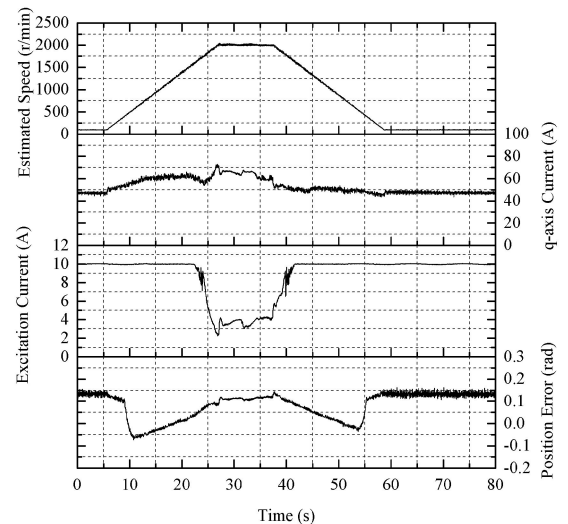


Fig. 12. Speed sensor fault-tolerant operation from 100 r/min to 2000 r/min, then back to 100 r/min with 50 % rated load.

Fig. 12 presents the performance of the CPPM machine operating in speed sensor fault condition. A slope speed reference of 100 r/min, 2000 r/min, and 100 r/min, is applied with 50 % rated load respectively. The speed response indicates a smooth transition between the two methods. The experimental results confirm that the reliability and continuous operation capability of the drive system is enhanced in the entire speed region when the speed sensor FTC is applied.

V. CONCLUSIONS

This paper proposes a speed sensor FTC strategy for EVs using a CPPM machine-based drive system. The HF voltage injection method and the extended-EMF method are combined to track the rotor position when the speed sensor failure is detected. The magnetic saliency of the CPPM machine is analysed by the FEA method and confirmed by measurement of a CPPM machine. The proposed speed sensor FTC strategy has been confirmed by the experimental results. High dynamics and a smooth transition could be guaranteed when the speed sensor failure occurs.

REFERENCES

- [1] I. Ozawa, T. Kosaka, N. Matsui, "Less rare-earth magnet-high power density hybrid excitation motor designed for hybrid electric vehicle drives", in *Proc. 13th Eur. Conf. Power Electron. Appl. (EPE'09)*, 2009, pp. 1–10.
- [2] J. A. Tapia, F. Leonardi, T. A. Lipo, "Consequent-pole permanent-magnet machine with extended field-weakening capability", *IEEE Trans. Industry Appl.*, vol. 39, no. 6, pp. 1704–1709, 2003. [Online]. Available: <http://dx.doi.org/10.1109/TIA.2003.818993>
- [3] T. Mizuno, K. Nagayama, T. Ashikaga, T. Kobayashi, "Basic principles and characteristics of hybrid excitation synchronous machine", *Elect. Eng. Jpn.*, vol. 117, no.5, pp. 110–123, 1996. [Online]. Available: <http://dx.doi.org/10.1002/ej.4391170510>
- [4] N. Patin, L. Vido, E. Monmasson, J. P. Louis, M. Gabsi, M. Lecrivain, "Control of a Hybrid Excitation Synchronous Generator for Aircraft Applications", *IEEE Trans. Ind. Electron.*, vol. 55, no. 10, pp. 3772–3783, 2008. [Online]. Available: <http://dx.doi.org/10.1109/TIE.2008.924030>
- [5] Y. Amara, L. Vido, M. Gabsi, E. Hoang, A. Hamid Ben Ahmed, M. Lecrivain, "Hybrid Excitation Synchronous Machines: Energy-Efficient Solution for Vehicles Propulsion", *IEEE Trans. Veh. Technol.*, vol. 58, no. 5, pp. 2137–2149, 2009. [Online]. Available: <http://dx.doi.org/10.1109/TVT.2008.2009306>
- [6] P. Brandstetter, T. Kreck, "Sensorless Control of Permanent Magnet Synchronous Motor Using Voltage Signal Injection", *Elektronika Ir Elektrotechnika*, vol. 19, no. 6, pp. 19–24, 2013. [Online]. Available: <http://dx.doi.org/10.5755/j01.eee.19.6.1583>
- [7] X. Z. Li Qin, Pengju Cao, "New Control Strategy for PMSM Driven Bucket Wheel Reclaimers using GA-RBF Neural Network and Sliding Mode Control", *Elektronika Ir Elektrotechnika*, no. 6, pp. 113–116, 2012.
- [8] B. Tabbache, M. E. H. Benbouzid, A. Kheloui, J. Bourgeot, "Virtual-Sensor-Based Maximum-Likelihood Voting Approach for Fault-Tolerant Control of Electric Vehicle Powertrains", *IEEE Trans. Veh. Technol.*, vol. 62, no. 3, pp. 1075–1083, 2013. [Online]. Available: <http://dx.doi.org/10.1109/TVT.2012.2230200>
- [9] M. Hasegawa, S. Yoshioka, K. Matsui, "Position Sensorless Control of Interior Permanent Magnet Synchronous Motors Using Unknown Input Observer for High-Speed Drives", *IEEE Trans. Ind. Appl.*, vol. 45, no. 3, pp. 938–946, 2009. [Online]. Available: <http://dx.doi.org/10.1109/TIA.2009.2018968>
- [10] D. Diallo, M. E. H. Benbouzid, A. Makouf, "A fault-tolerant control architecture for induction motor drives in automotive applications", *IEEE Trans. Veh. Technol.*, vol. 53, no. 6, pp. 1847–1855, 2004. [Online]. Available: <http://dx.doi.org/10.1109/TVT.2004.833610>
- [11] G. H. B. Foo, Z. Xinan, D. M. Vilathgamuwa, "A Sensor Fault Detection and Isolation Method in Interior Permanent-Magnet Synchronous Motor Drives Based on an Extended Kalman Filter", *IEEE Trans. Ind. Electron.*, vol. 60, no. 8, pp. 3485–3495, 2013. [Online]. Available: <http://dx.doi.org/10.1109/TIE.2013.2244537>
- [12] S. M. Taghavi, M. Jain, S. S. Williamson, "A comparative study of sensorless control techniques of interior permanent magnet synchronous motor drives for electric vehicles", in *Proc. Veh. Power Propulsion*, Chicago, 2011, pp. 1–7.
- [13] Z. Li, Y. Li, X. Li, "Flux Control of a CPPM Machine for Both a Wide Speed Range and High Efficiency", *IEEE Trans. Power Electron.*, (to be published).
- [14] J. Yu-Seok, S. Seung-Ki, S. E. Schulz, N. R. Patel, "Fault detection and fault-tolerant control of interior permanent-magnet motor drive system for electric vehicle", *IEEE Trans. Industry Appl.*, vol. 41, no. 1, pp. 46–51, 2005. [Online]. Available: <http://dx.doi.org/10.1109/TIA.2004.840947>
- [15] J. Ji-Hoon, H. Jung-Ik, M. Ohto, K. Ide, S. Seung-Ki, "Analysis of permanent-magnet machine for sensorless control based on high-frequency signal injection", *IEEE Trans. Industry Appl.*, vol. 40, no. 6, pp. 1595–1604, 2004. [Online]. Available: <http://dx.doi.org/10.1109/TIA.2004.836222>
- [16] J. Ji-Hoon, S. Seung-Ki, H. Jung-Ik, K. Ide, M. Sawamura, "Sensorless drive of surface-mounted permanent-magnet motor by high-frequency signal injection based on magnetic saliency", *IEEE Trans. Industry Appl.*, vol. 39, no. 4, pp. 1031–1039, 2003. [Online]. Available: <http://dx.doi.org/10.1109/TIA.2003.813734>
- [17] H. Jung-Ik, "Analysis of Inherent Magnetic Position Sensors in Symmetric AC Machines for Zero or Low Speed Sensorless Drives", *IEEE Trans. Magn.*, vol. 44, no. 12, pp. 4689–4696, 2008. [Online]. Available: <http://dx.doi.org/10.1109/TMAG.2008.2003479>